NASA TECHNICAL NOTE

NASA TN D-2785

LONGITUDINAL STABILITY CHARACTERISTICS OF SEVERAL PROPOSED PLANETARY ENTRY VEHICLES AT MACH 6.73

by Peter T. Bernot

Langley Research Center
Langley Station, Hampton, Va.

NATIONAL AERONAUTICS AND SPACE ADMINISTRATION • WASHINGTON, D. C. • APRIL 1965

NASA TN D-2785

LONGITUDINAL STABILITY CHARACTERISTICS OF SEVERAL PROPOSED PLANETARY ENTRY VEHICLES AT MACH 6.73

By Peter T. Bernot

Langley Research Center
Langley Station, Hampton, Va.

NATIONAL AERONAUTICS AND SPACE ADMINISTRATION

For sale by the Clearinghouse for Federal Scientific and Technical Information
Springfield, Virginia 22151 – Price $1.00

LONGITUDINAL STABILITY CHARACTERISTICS OF SEVERAL PROPOSED PLANETARY ENTRY VEHICLES AT MACH 6.73

By Peter T. Bernot
Langley Research Center

SUMMARY

Aerodynamic characteristics of several planetary entry vehicles with different nose-bluntness ratios were obtained over an angle-of-attack range from 0° to 140° at a Mach number of 6.73 and at Reynolds numbers of 0.19×10^6 and 0.25×10^6. At an angle of attack of 0°, the flow about these configurations was characterized by large-scale flow separation accompanied by shock-wave fluctuations, notably for the sharp-nose model. As angle of attack was increased to about 10°, this separated-flow region on the windward side of the model was swept aside with the result that large increases occurred in normal and axial force and in pitching moment. A high level of positive stability was obtained for all the models at an angle of attack of 0°; for the tests at angles of attack greater than 90°, the models showed no additional stable trim points. Positive stability was maintained for all models near an angle of attack of 0° as center-of-gravity location was varied longitudinally from 20 to 90 percent of the body length from the nose. Varying the location of the center of gravity along the vertical axis as much as 7.5 percent of the base diameter resulted in small changes in trim angle of attack. Increasing the nose-bluntness ratio decreased the axial-force coefficient and the stability.

INTRODUCTION

Much attention is now being given to unmanned vehicles suitable for entry into planetary atmospheres. A primary mission of such a vehicle would be to experimentally determine characteristics of the subject atmosphere. Reference 1 presents several methods for determining atmospheric properties of Mars and Venus from the dynamic behavior of a probe vehicle whose aerodynamic characteristics are known. Inasmuch as a long entry time is desired to facilitate the accumulation and transmittal of measured data, the vehicle should have a low value of ballistic parameter and be aerodynamically stable.

A series of model configurations, evolved from structural concepts (ref. 2), are presently under investigation at the Langley Research Center. In these designs, nose bluntness is dictated by payload geometry and aerodynamic heating, and the base is large because of the need to achieve high drag. In order to minimize vehicle weight, the base and payload are connected by a relatively light membrane capable of withstanding high temperatures.

The purpose of this paper is to present hypersonic longitudinal characteristics of several of these configurations. Four models were tested at a Mach number of 6.73 in air over an angle-of-attack range from 0° to 140°. Normal and axial forces as well as pitching moments were measured by a strain-gage balance. Newtonian estimates are also included. Reynolds numbers, based on model-base diameter, were 0.19×10^6 and 0.25×10^6.

SYMBOLS

The data are referred to the body system of axes originating at a center of gravity located at a station 25 percent of the base diameter from the base and, unless otherwise noted, on the model center line. (See figs. 1 and 2.)

A	reference area, $\pi D^2/4$
C_A	axial-force coefficient, $\frac{\text{Axial force}}{qA}$
C_N	normal-force coefficient, $\frac{\text{Normal force}}{qA}$
C_m	pitching-moment coefficient, $\frac{\text{Pitching moment}}{qAD}$
C_{m_α}	stability parameter, $\partial C_m/\partial\alpha$ at $\alpha = 0°$, per deg
C_p	pressure coefficient
D	model-base diameter
l	model length
M	free-stream Mach number
q	dynamic pressure
r	radial coordinate
r_n	nose radius
X,Z	body-axis system (fig. 1)
x,z	model coordinates
α	angle of attack, deg

Subscript:

max maximum

APPARATUS, MODELS, AND TEST CONDITIONS

This investigation was conducted in the Langley 11-inch hypersonic tunnel, which is a blowdown-to-vacuum type of tunnel. A two-dimensional, contoured nozzle fabricated from invar was used to produce a Mach number slightly under 7. To avoid liquefaction, dried air was passed through an electrically heated bundle of high-temperature tubes. A more detailed description of this facility and of nozzle calibrations may be found in references 3 and 4.

Stagnation temperature was measured by a chromel-alumel thermocouple whose output was recorded on a strip-chart potentiometer, and stagnation pressure was determined by a Bourdon-type gage. Angle of attack was measured optically by reflecting a light beam off a small prism that was mounted in the shielded region of the model. A six-component strain-gage balance was used in conjunction with strip-chart potentiometers to measure model forces and moments. A circular wind shield of 0.70-inch diameter provided protection to the balance from the airstream. Measurements of windshield chamber pressures were made by use of a bellows-type instrument. This facility is equipped with a schlieren system that has a vertical Z-shape light path in conjunction with a horizontal knife edge.

Dimensions of the four models in this investigation are shown in figure 2. Models 1, 2, and 3 have the same planform contour but different nose-bluntness ratios; model 4 differs in planform contour from the other three models but has about the same nose-bluntness ratio as model 3. Two-inch-diameter, base-supported models were machined from stainless steel for the investigation in the angle-of-attack range from 0° to 70°. For the investigation at angles of attack from 90° to 140°, larger models of 2 and 4 (base diameters of 3 inches) were fabricated for side mounting in order to reduce sting-interference effects. Photographs of all the models are presented in figure 3. For the tests at angles of attack from 0° to 70°, the average stagnation pressure was 7.5 atmospheres absolute; the average stagnation temperature was 685° F; and the resulting Reynolds number, based on model diameter, was 0.19×10^6. For angles of attack exceeding 90°, the corresponding average values of pressure, temperature, and Reynolds number were 7.9 atmospheres absolute, 670° F, and 0.25×10^6. Average Mach number was 6.73. Each test run had a duration of about 55 seconds. Schlieren photographs were obtained during the investigation by use of the flash technique.

ACCURACY

An estimate of maximum balance error is based on 0.5 percent of the maximum design load of each component. This estimated error, expressed in coefficient form, is as follows:

	For $\alpha = 0^\circ$ to 70°	For $\alpha = 90^\circ$ to 140°
C_N	±0.024	±0.006
C_A	±0.015	±0.010
C_m	±0.017	±0.004

The Mach number was accurate within ±0.04. Maximum error in angle of attack was ±0.10°. The axial-force data were corrected to a windshield pressure equal to free-stream static pressure applied to the windshield area only. The corrections for the axial-force data were always small and were calculated only for the investigation in the angle-of-attack range from 0° to 70°.

DISCUSSION OF RESULTS

General Flow Field

Schlieren photographs of the flow about each model at an angle of attack of 0° are shown in figure 4. The basic shock structure shows a bow shock intersecting the detached wave which originates ahead of the flared skirt where the body slope exceeds the maximum turning that the stream can support. These photographs shown in figure 4 were taken at 8- or 9-second intervals. Shock instability, evident on all models, is especially noticeable on model 1 which has zero nose bluntness; increased nose bluntness reduces the shock fluctuations. No attempt was made to measure the strength or frequency of these fluctuations. Similar shock instability on models having concave surfaces has been reported in reference 5.

The photographs of the models at $\alpha = 0^\circ$ shown in figure 4 indicate a region of separated flow that engulfs each model and thus drastically changes the effective model shape. For instance, for the sharp-nose model 1, which has a geometric body slope of 20° at the nose, the measured angle of the separated region is about 35°; the measured shock-wave angle is 40° and is in good agreement with ideal-flow values for cones. The extent of the separated region is shown in reference 5 to vary with wall temperature of the model. For example, at a wall-temperature to stagnation-temperature ratio of 0.25, the shadow photographs in reference 5 showed attached flow for those models having essentially zero nose bluntness; whereas increasing the temperature ratio to 0.50 or greater resulted in large-scale separation. The lowest value of temperature ratio in the present investigation was about 0.50. The schlieren photographs in figure 4 show large-scale separation at the beginning of the test with no major changes in shock-wave pattern as wall temperatures of the models increased during the course of the test run.

In figure 5, schlieren photographs are presented for the entire angle-of-attack range covered in the investigation of the models. Movement of the bow shock closer to the model with increasing angle of attack is indicative of reduced separation as the boundary layer was swept from the windward side. As the angle of attack of the model is increased beyond 10°, the rear shock wave

moves forward on the windward surface and merges with the front shock wave at an angle of attack of 50°. No flow separation in the nose region is evident at this angle of attack for any of the models. It is noted that the shock wave that impinges on the balance shield moves closer to the model as angle of attack increases to 70°; this situation could influence the base pressure and hence the measured axial forces. Only models 2 and 4 were investigated over an angle-of-attack range from 90° to 140° and, in general, the same flow pattern is exhibited by both shapes.

Longitudinal Characteristics

The longitudinal stability characteristics of the models are presented in figure 6. Included in the figure are Newtonian estimates for models 1, 2, and 3 over an angle-of-attack range from 0° to 90°. These force- and moment-coefficient predictions were obtained by means of an electronic computer that incorporated a calculation procedure based on the method described in reference 6. A value of $C_{p,max}$ of 2.00 was used in these calculations. The Newtonian pitching-moment coefficients include the incremental moment contributed by the axial force. Secondary shielding effects caused by the nose were neglected.

The trends of the experimental data are generally consistent with the theory except in the low angle-of-attack range where with increasing angle of attack, the region of separated flow gave way to the attached flow on the windward side of the model. Both normal- and axial-force coefficients show rapid increases up to an angle of attack of about 10°. (See fig. 6.) Maximum values of normal-force coefficient are obtained near an angle of attack of 60°, and this result is fairly well predicted by theory. Maximum values of axial-force coefficient are seen to occur near an angle of attack of 10°. In the high angle-of-attack range, the normal-force coefficients for models 2 and 4 are seen to merge with those data obtained at $M = 6.8$ for the circular wing (flat-plate disk) in reference 7; however, some disagreement is noted at an angle of attack of 140° for the axial-force data. This difference between the two sets of axial-force data may be associated with flow reattachment on the afterbody of the models in the present investigation. (See fig. 5.) With the center of gravity located on the model center line at a station 25 percent of the base diameter from the model base, all models exhibit high levels of stability at a trim angle of attack of 0°. The sharp break in the pitching-moment curves at angles of attack from 6° to 10° coincides with the appearance of normal shocks just ahead of the flare on the upper surface of the models as shown in the schlieren photographs of figure 5. The data in figure 6 show unstable trim points for models 2 and 4 at angles of attack of about 123° and 128°, respectively.

Effect of nose-bluntness ratio on longitudinal characteristics is presented in figure 7. Although the Newtonian theory predicts an increase in axial-force coefficient with increasing bluntness at an angle of attack of 0°, the experimental data show that the model with zero nose bluntness (model 1) had the largest axial-force coefficient. Reasonably good agreement with theory was obtained for models 2 and 3; however, in view of the complex viscous flow involved, this result is considered fortuitous. Model 4, which has the largest cross-sectional area relative to the base area, shows a much smaller axial-force coefficient

than does model 3, which has nearly the same nose-bluntness ratio. When the angle of attack is changed from 0° to 10°, the increase in measured axial-force coefficient amounts to 23 percent for model 1, 33 percent for models 2 and 3, and 50 percent for model 4.

An almost linear decrease in the stability $(-C_{m_\alpha})$ occurs as nose-bluntness ratio is increased. The greater stability of the longer models is associated with increased loading due to more efficient compression along the windward flared portion of the models. Figure 7 shows that model 4 possesses about the same stability as model 3.

The change in pitching-moment coefficient effected by varying the location of the center of gravity along the longitudinal axis is presented in figure 8. With the center-of-gravity location varied from 20 to 90 percent of the model length (measured from the nose), positive stability was maintained for the models near an angle of attack of 0°. Because much attention is now being given to reentry vehicles having lift-drag ratios greater than zero, the effect of varying the center-of-gravity location along the Z-axis is also investigated and is presented in figure 9. With the center of gravity located on the vertical axis at a station 7.5 percent of the base diameter off the center line (measured from the center line at a point 0.25D from the base), stable trim points range from an angle of attack of 2° for model 1 to an angle of attack of 5° for model 3. This result indicates that nose bluntness has an effect in determining trim points. For this same center-of-gravity location, the figure shows that model 1 has an additional stable trim point at an angle of attack of about 30° whereas models 2 and 3 have essentially neutral stability near an angle of attack of 20°. With the center of gravity located on the vertical axis at a station 5 percent of the base diameter off the center line, only model 1 shows a second stable trim point (near an angle of attack of 24°).

CONCLUDING REMARKS

Aerodynamic characteristics of several entry vehicles with different nose-bluntness ratios were obtained at a Mach number of 6.73 over an angle-of-attack range from 0° to 140°. At an angle of attack of 0°, the flow about these configurations was characterized by large-scale flow separation accompanied by shock-wave fluctuations, notably for the sharp-nose model. As angle of attack was increased to about 10°, this separated region on the windward side of the model was swept aside with the result that large increases occurred in normal and axial force and in pitching moment. A high level of positive stability was obtained for all the models at an angle of attack of 0°; for the tests at angles of attack greater than 90°, the models showed no additional stable trim points. Positive stability was maintained for all models near an angle of attack of 0° as center-of-gravity location was varied longitudinally from 20 to 90 percent of the body length. Varying the center-of-gravity location along the vertical axis from 0 to 7.5 percent of body-base diameter (measured from the center line at a station 25 percent of the base diameter from the model base) resulted in small changes in trim angle of attack and in the introduction of additional trim

points at higher angles of attack ($\alpha = 24^{\circ}$ and 30°). Increasing nose-bluntness ratio decreased the axial-force coefficient and the stability.

Langley Research Center,
National Aeronautics and Space Administration,
Langley Station, Hampton, Va., February 11, 1965.

REFERENCES

1. Seiff, Alvin: Some Possibilities for Determining the Characteristics of the Atmospheres of Mars and Venus From Gas-Dynamic Behavior of a Probe Vehicle. NASA TN D-1770, 1963.

2. Anderson, Melvin S.; Robinson, James C.; Bush, Harold G.; and Fralich, Robert W.: A Tension Shell Structure for Application to Entry Vehicles. NASA TN D-2675, 1965.

3. McLellan, Charles H.; Williams, Thomas W.; and Bertram, Mitchel H.: Investigation of a Two-Step Nozzle in the Langley 11-Inch Hypersonic Tunnel. NACA TN 2171, 1950.

4. Bertram, Mitchel H.: Exploratory Investigation of Boundary-Layer Transition on a Hollow Cylinder at a Mach Number of 6.9. NACA Rep. 1313, 1957. (Supersedes NACA TN 3546.)

5. Centolanzi, Frank J.: Heat Transfer to Blunt Conical Bodies Having Cavities to Promote Separation. NASA TN D-1975, 1963.

6. Rainey, Robert W.: Working Charts for Rapid Prediction of Force and Pressure Coefficients on Arbitrary Bodies of Revolution by Use of Newtonian Concepts. NASA TN D-176, 1959.

7. Penland, Jim A.; and Armstrong, William O.: Static Longitudinal Aerodynamic Characteristics of Several Wing and Blunt-Body Shapes Applicable for Use as Reentry Configurations at a Mach Number of 6.8 and Angles of Attack up to 90°. NASA TM X-65, 1959.

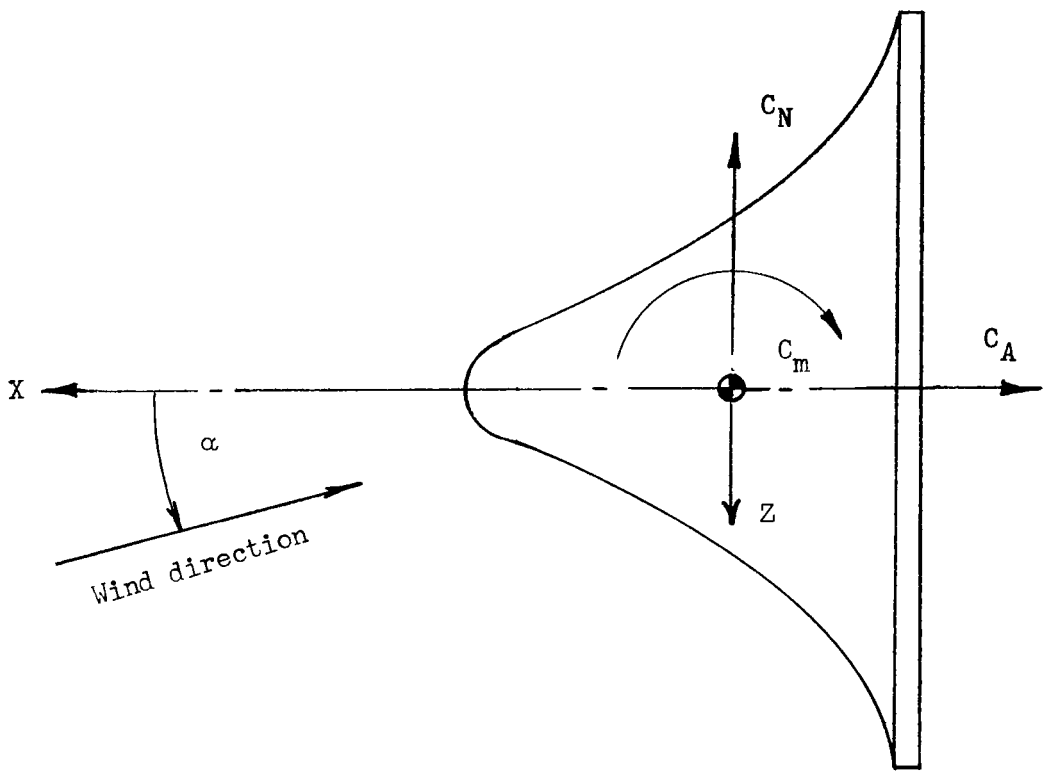

Figure 1.- Body-axis system. Arrows indicate positive directions.

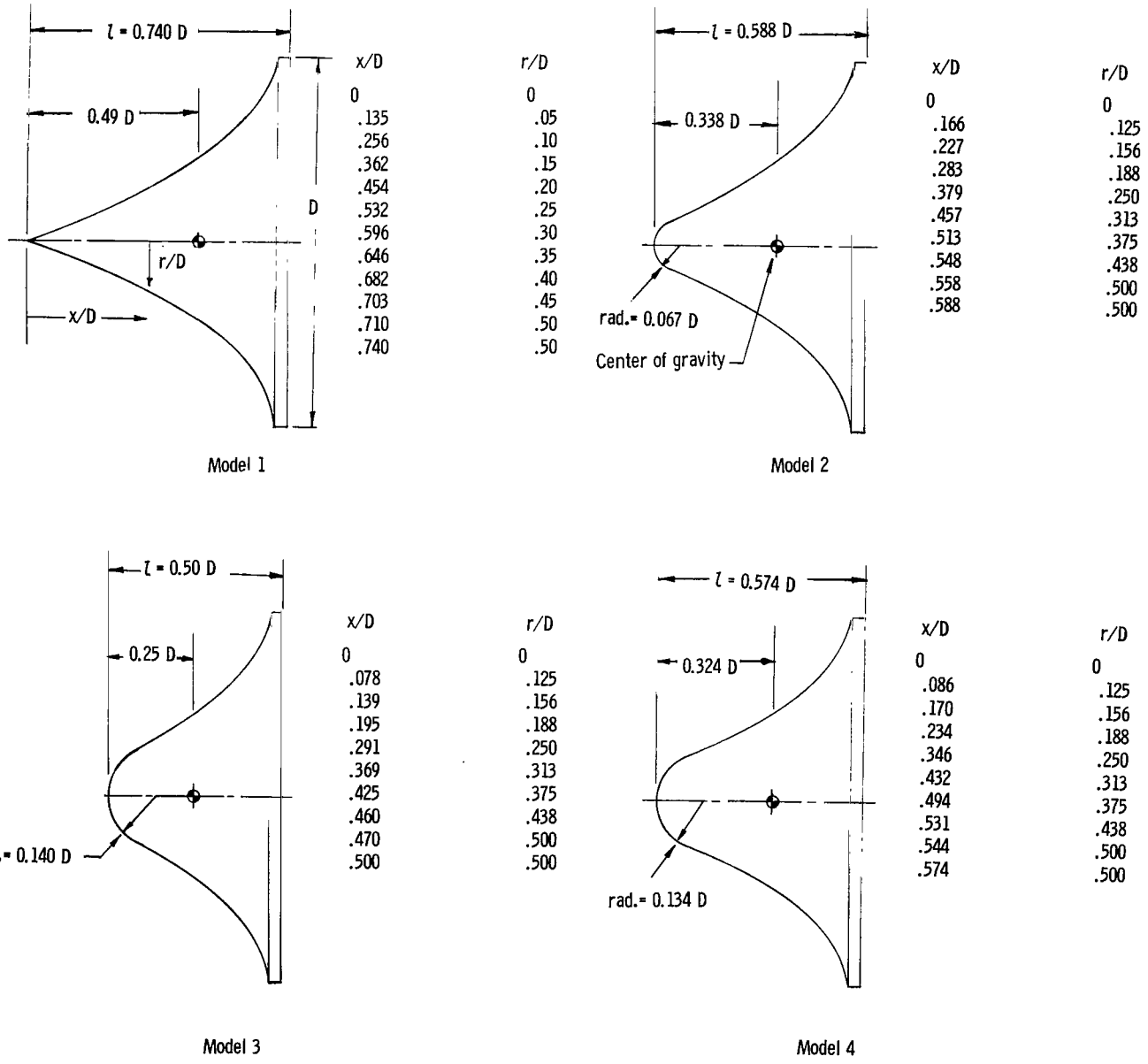

Figure 2.- Model details. The center of gravity is located at D/4 from the base for all models.

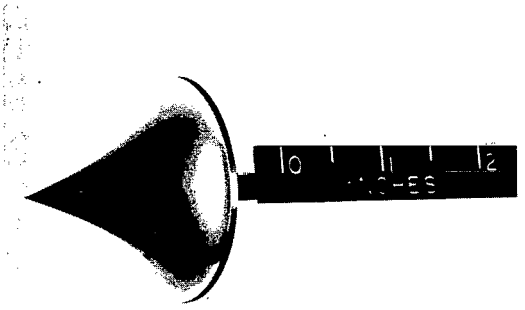

Model 1

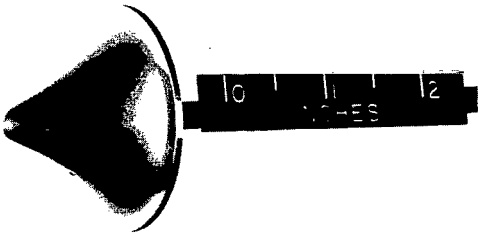

Model 2

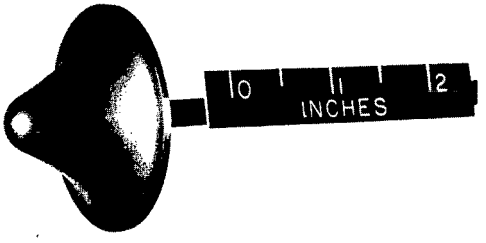

Model 3

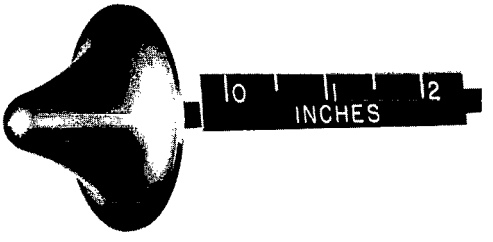

Model 4

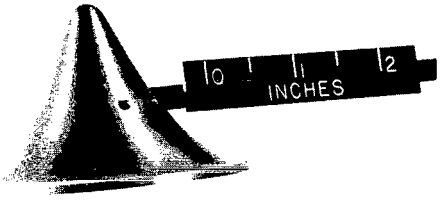

Model 2 (side-mounted)

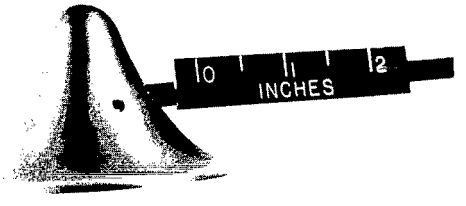

Model 4 (side-mounted)

Figure 3.- Photographs of models. L-65-17

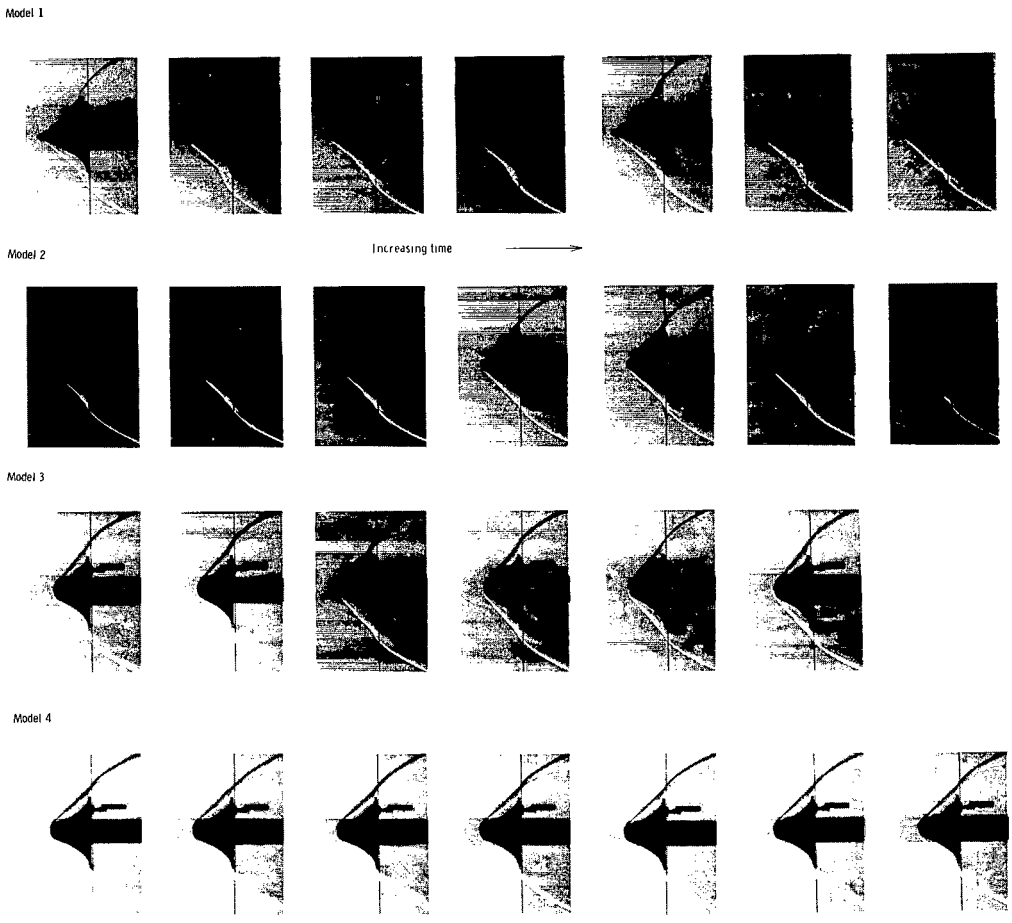

Figure 4.- Schlieren photographs of models at $\alpha = 0^{\circ}$. L-65-18

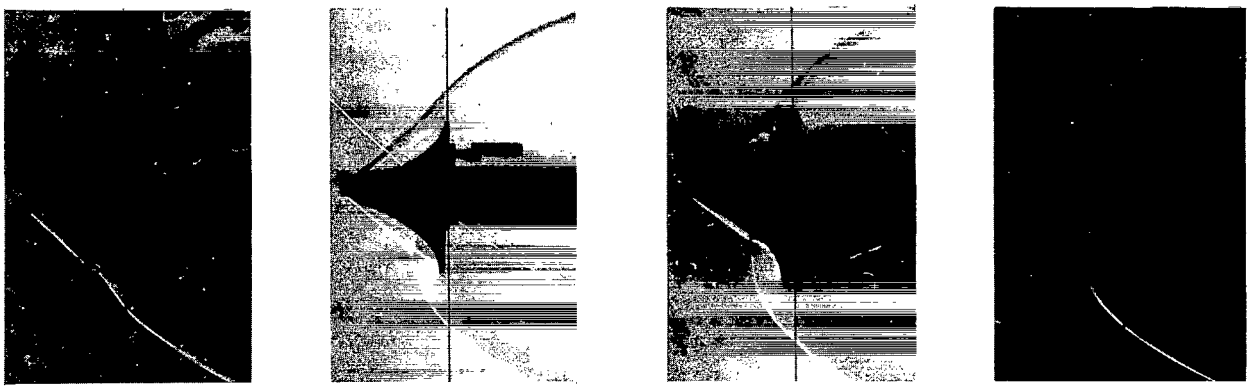

$\alpha = 0^\circ$ $\alpha = 3^\circ$ $\alpha = 6^\circ$ $\alpha = 10^\circ$

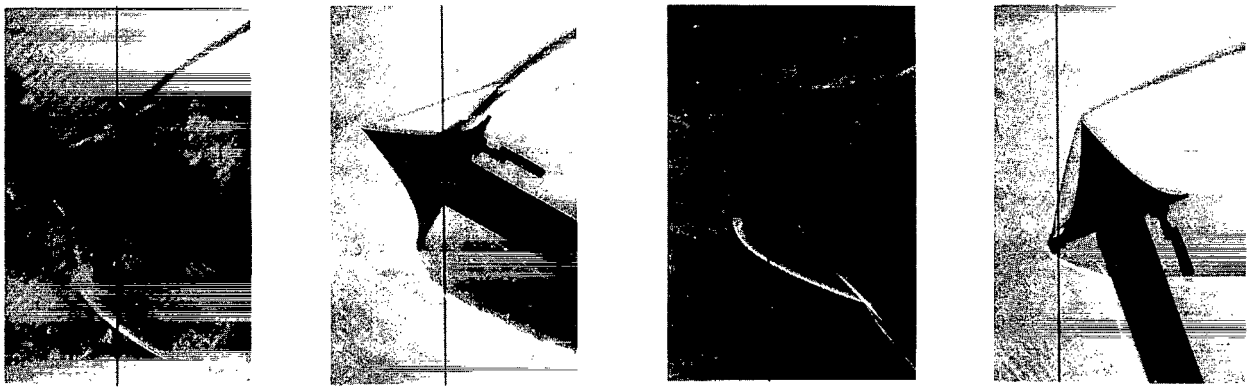

$\alpha = 20^\circ$ $\alpha = 30^\circ$ $\alpha = 50^\circ$ $\alpha = 70^\circ$

(a) Model 1.

L-65-19

Figure 5.- Schlieren photographs of models at various angles of attack.

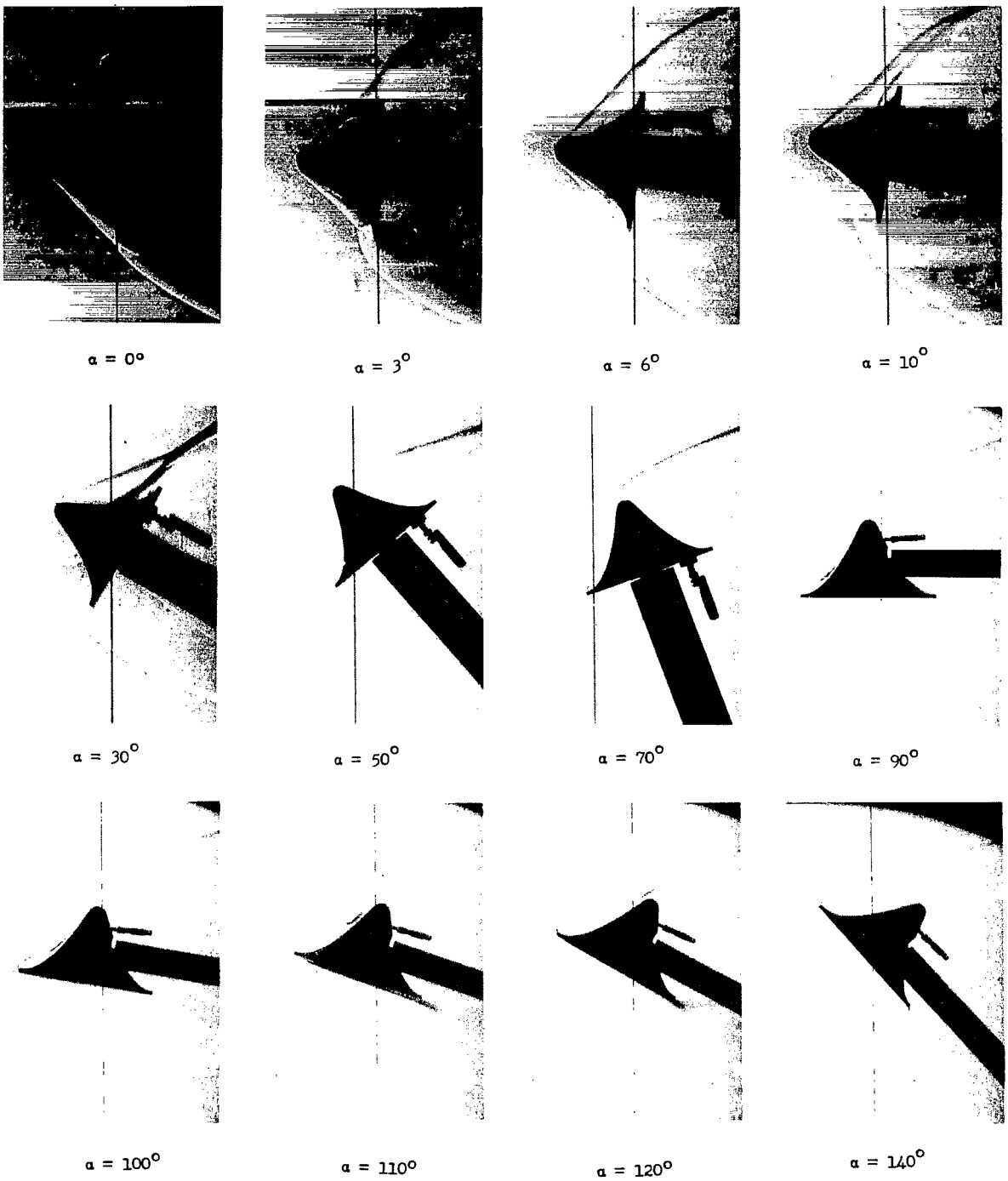

(b) Model 2. L-65-20

Figure 5.- Continued.

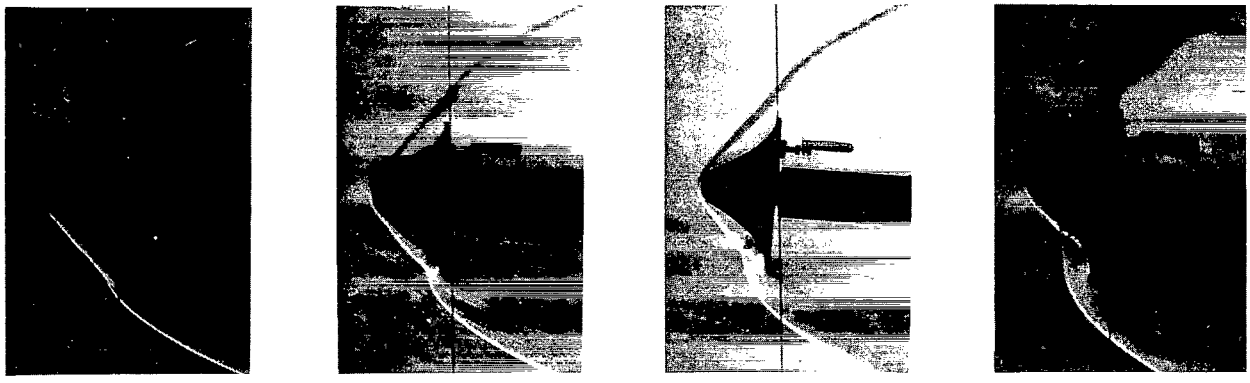

$\alpha = 0^\circ$ $\alpha = 3^\circ$ $\alpha = 6^\circ$ $\alpha = 10^\circ$

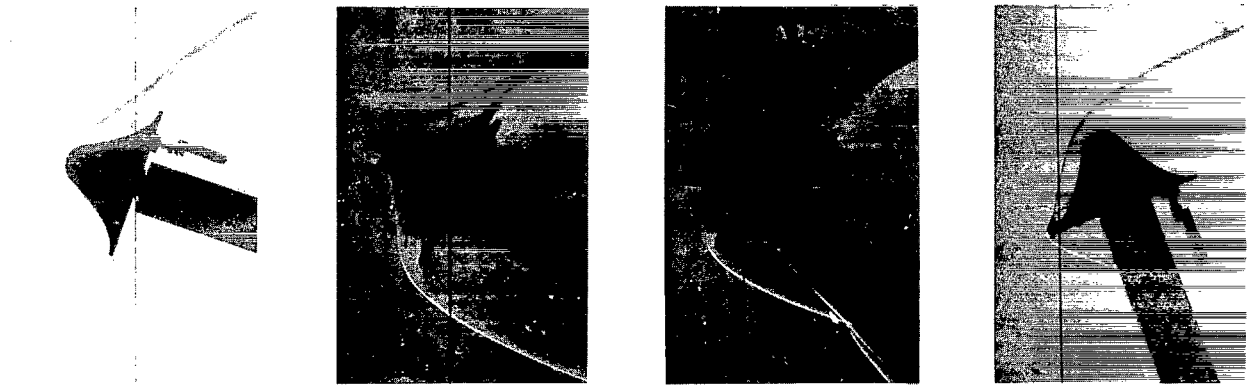

$\alpha = 20^\circ$ $\alpha = 30^\circ$ $\alpha = 50^\circ$ $\alpha = 70^\circ$

(c) Model 3. L-65-21

Figure 5.- Continued.

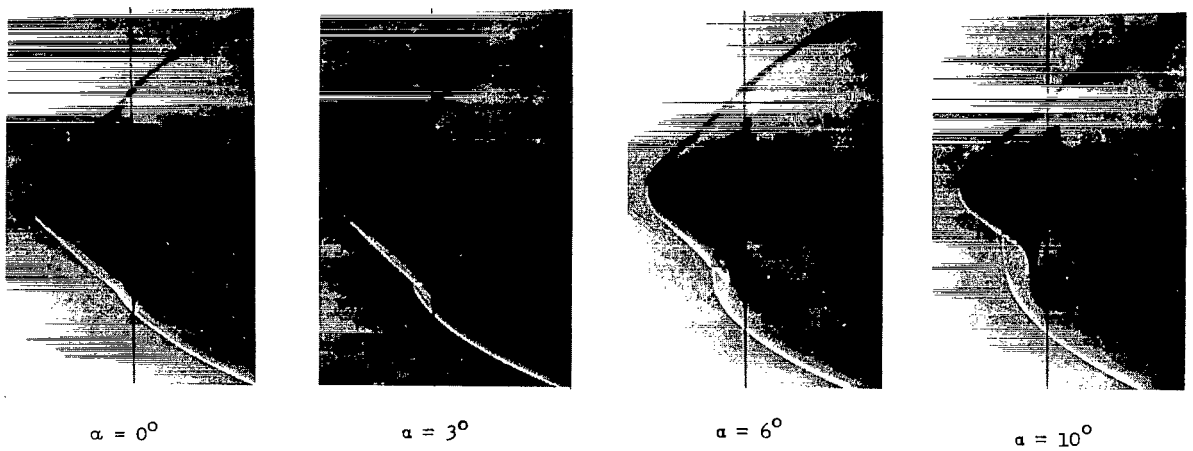

$\alpha = 0^\circ$ $\alpha = 3^\circ$ $\alpha = 6^\circ$ $\alpha = 10^\circ$

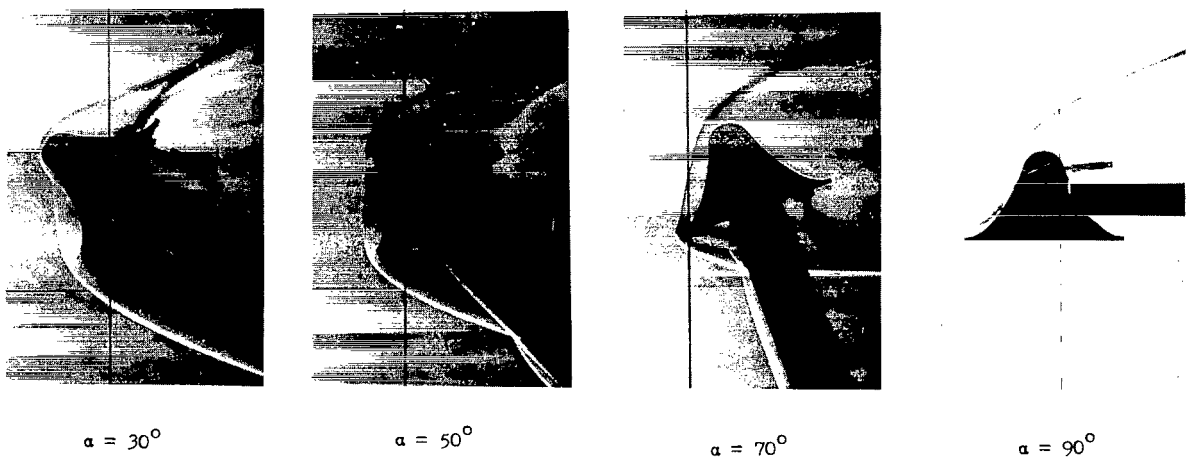

$\alpha = 30^\circ$ $\alpha = 50^\circ$ $\alpha = 70^\circ$ $\alpha = 90^\circ$

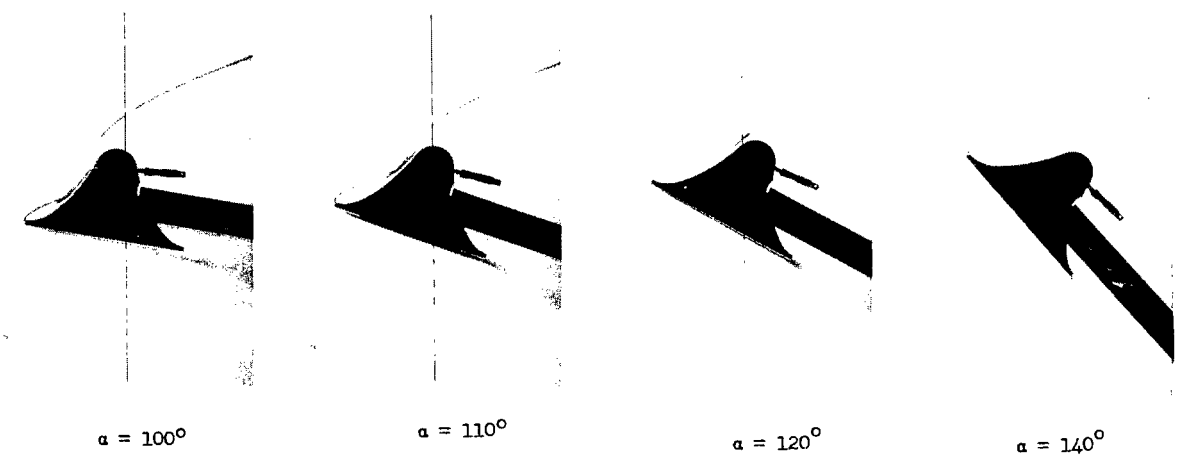

$\alpha = 100^\circ$ $\alpha = 110^\circ$ $\alpha = 120^\circ$ $\alpha = 140^\circ$

(d) Model 4.

L-65-22

Figure 5.- Concluded.

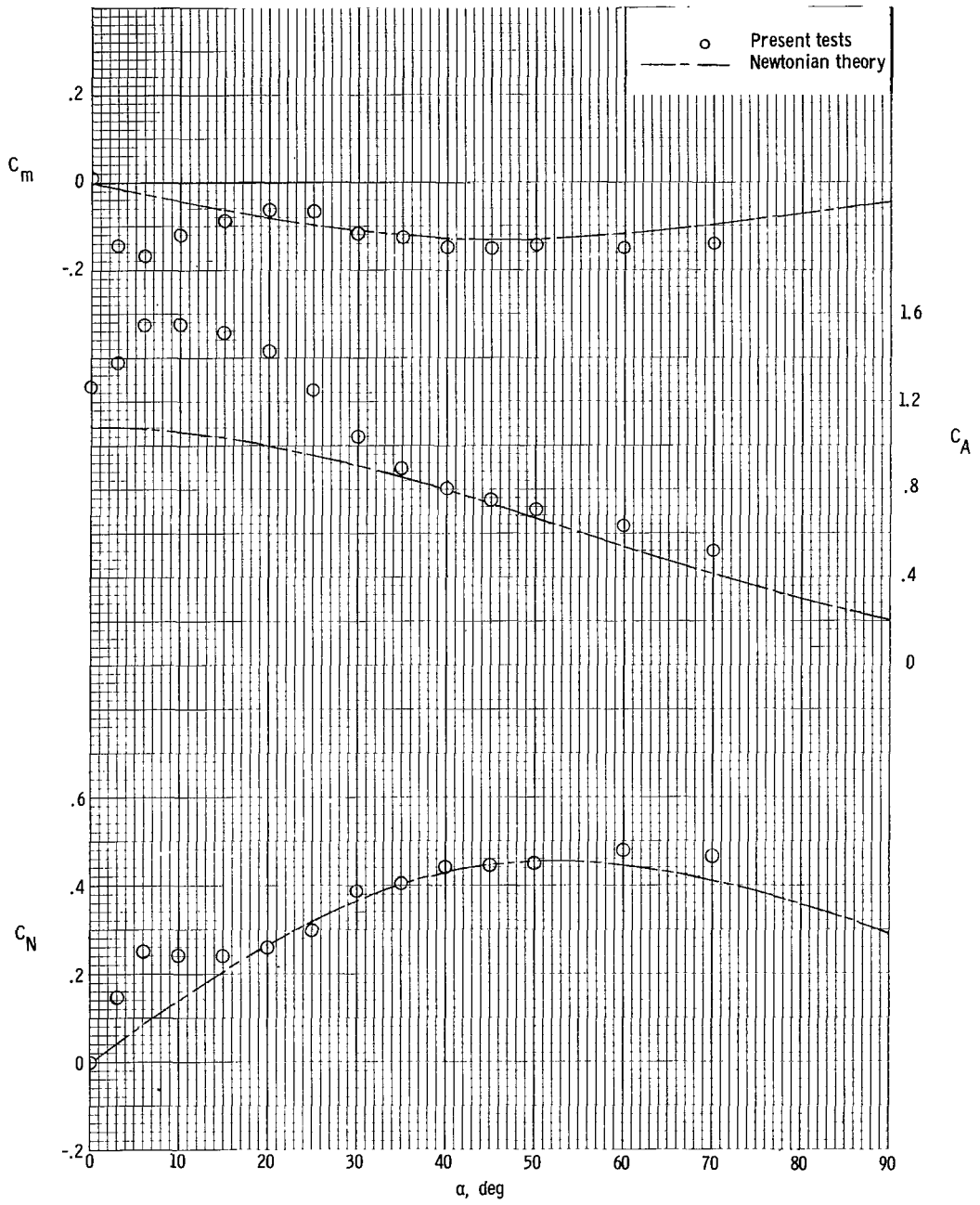

(a) Model 1.

Figure 6.- Longitudinal stability characteristics.

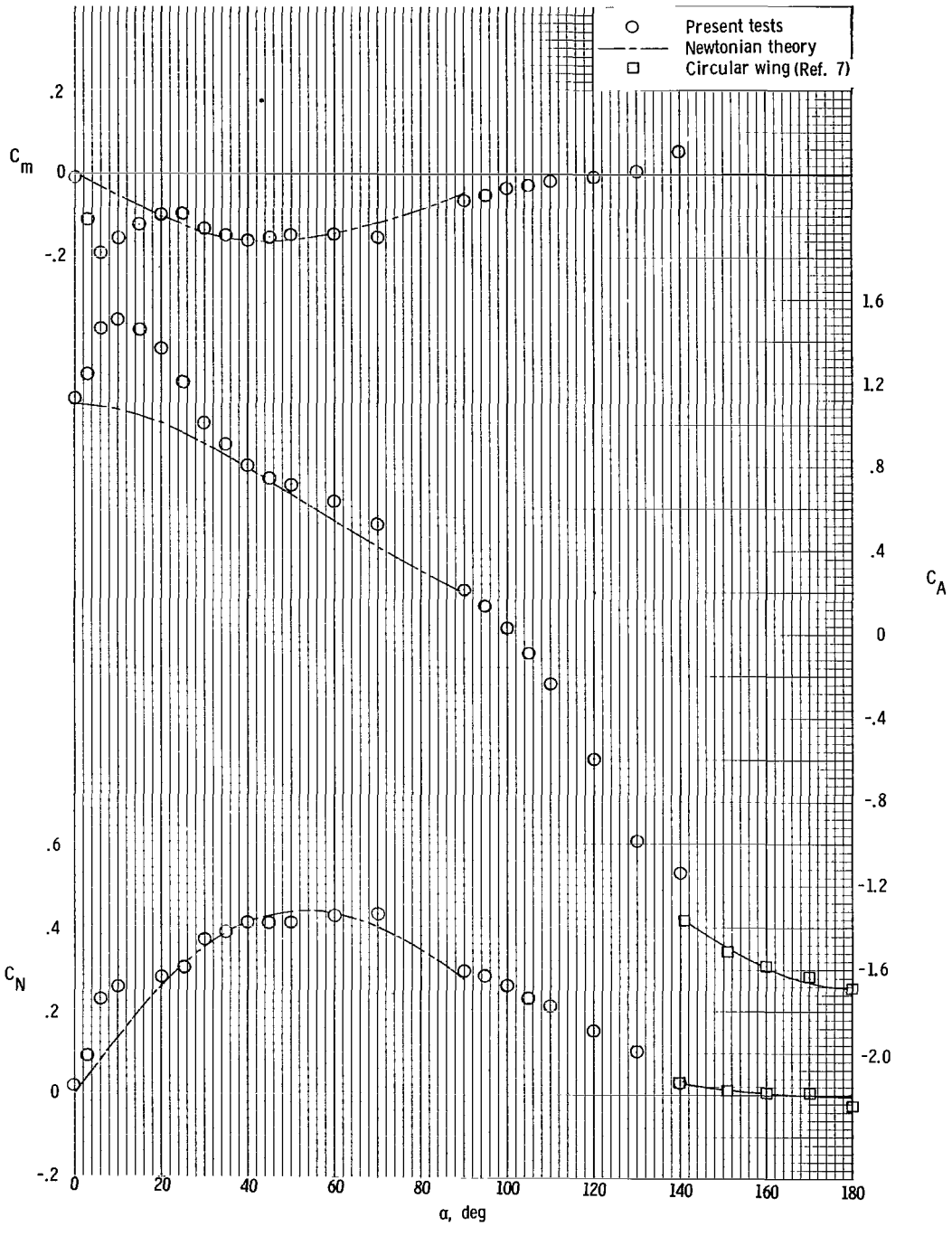

(b) Model 2.

Figure 6.- Continued.

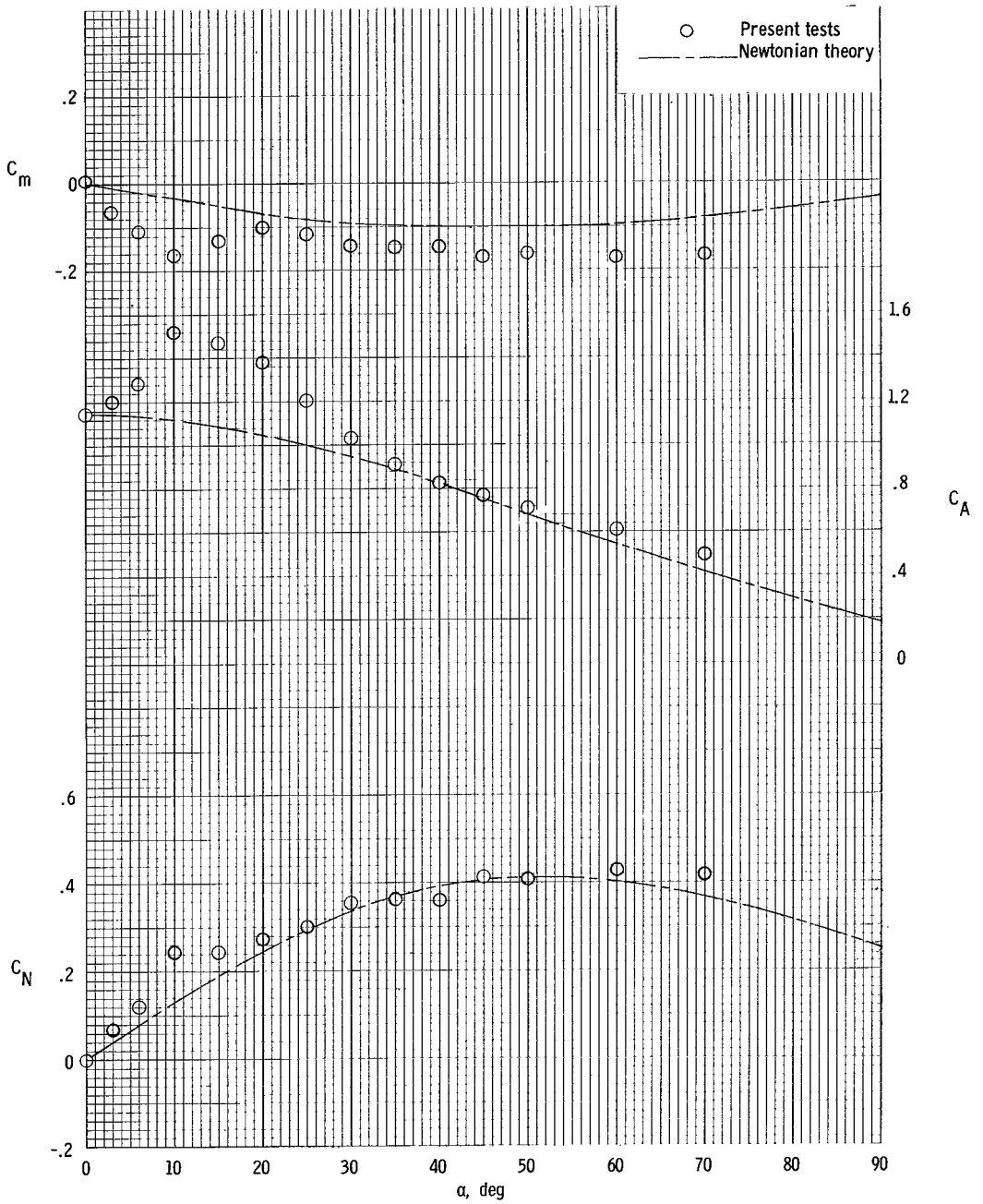

(c) Model 3.

Figure 6.- Continued.

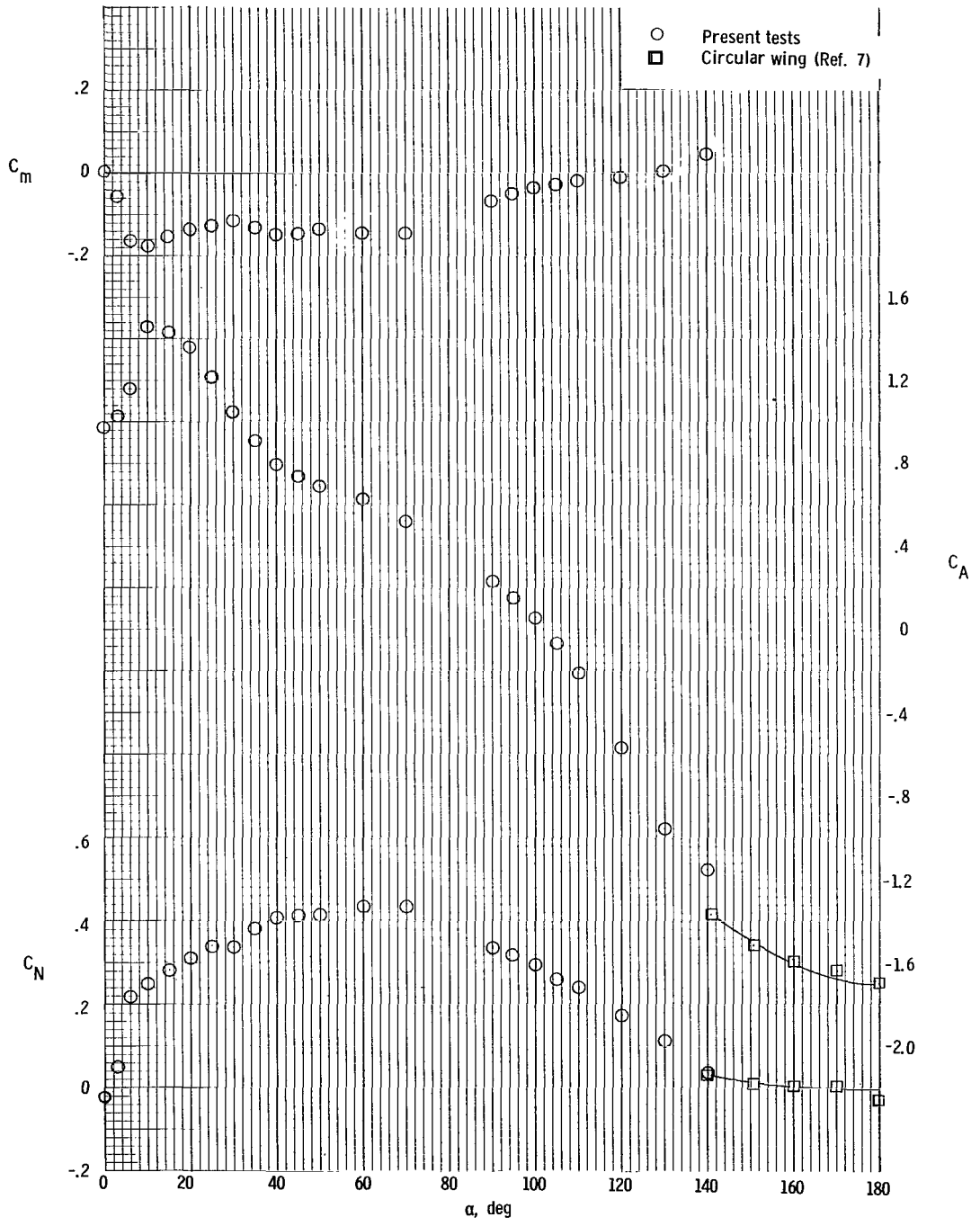

(d) Model 4.

Figure 6.- Concluded.

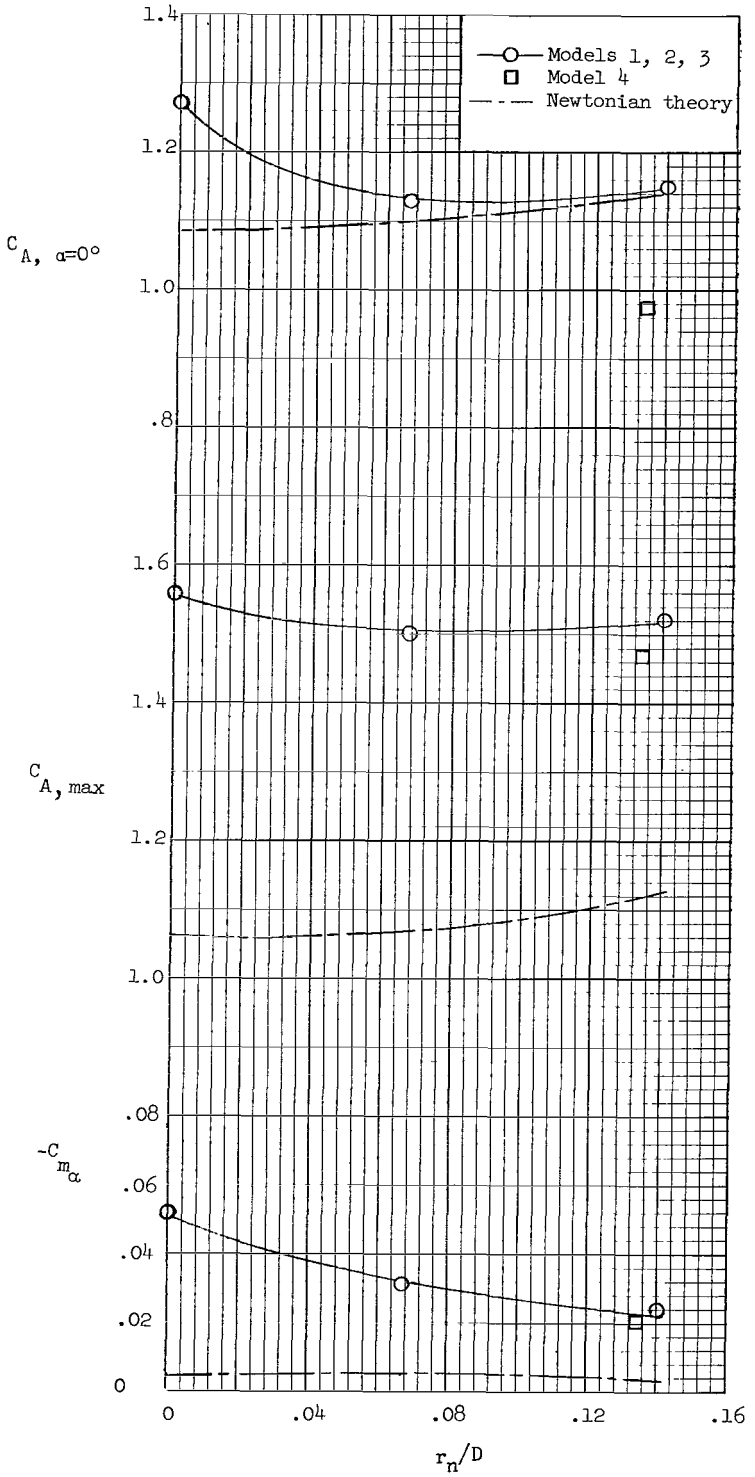

Figure 7.- Effect of nose-bluntness ratio on longitudinal stability characteristics.

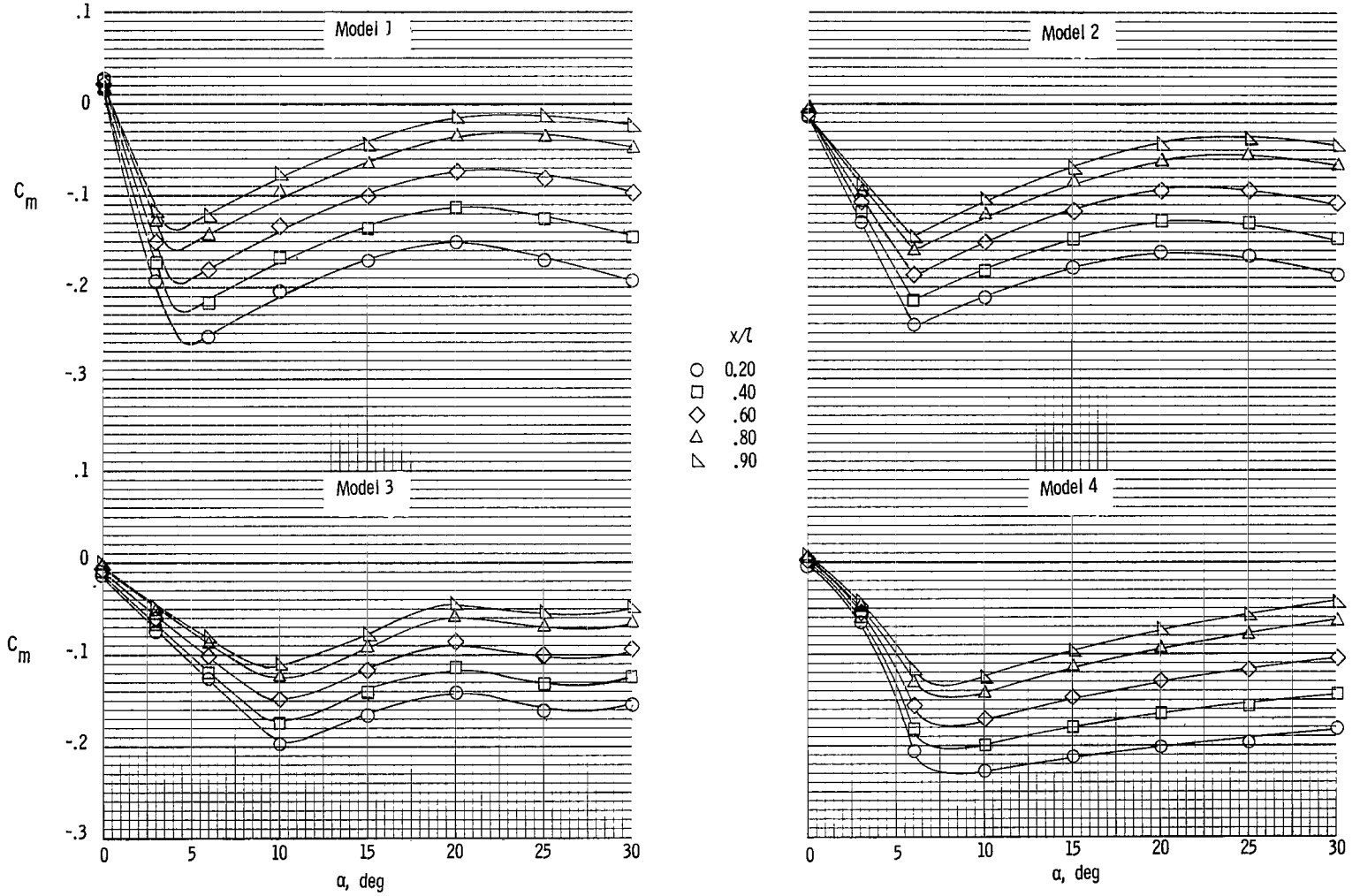

Figure 8.- Effect of varying center-of-gravity location along the longitudinal axis on pitching-moment coefficient.

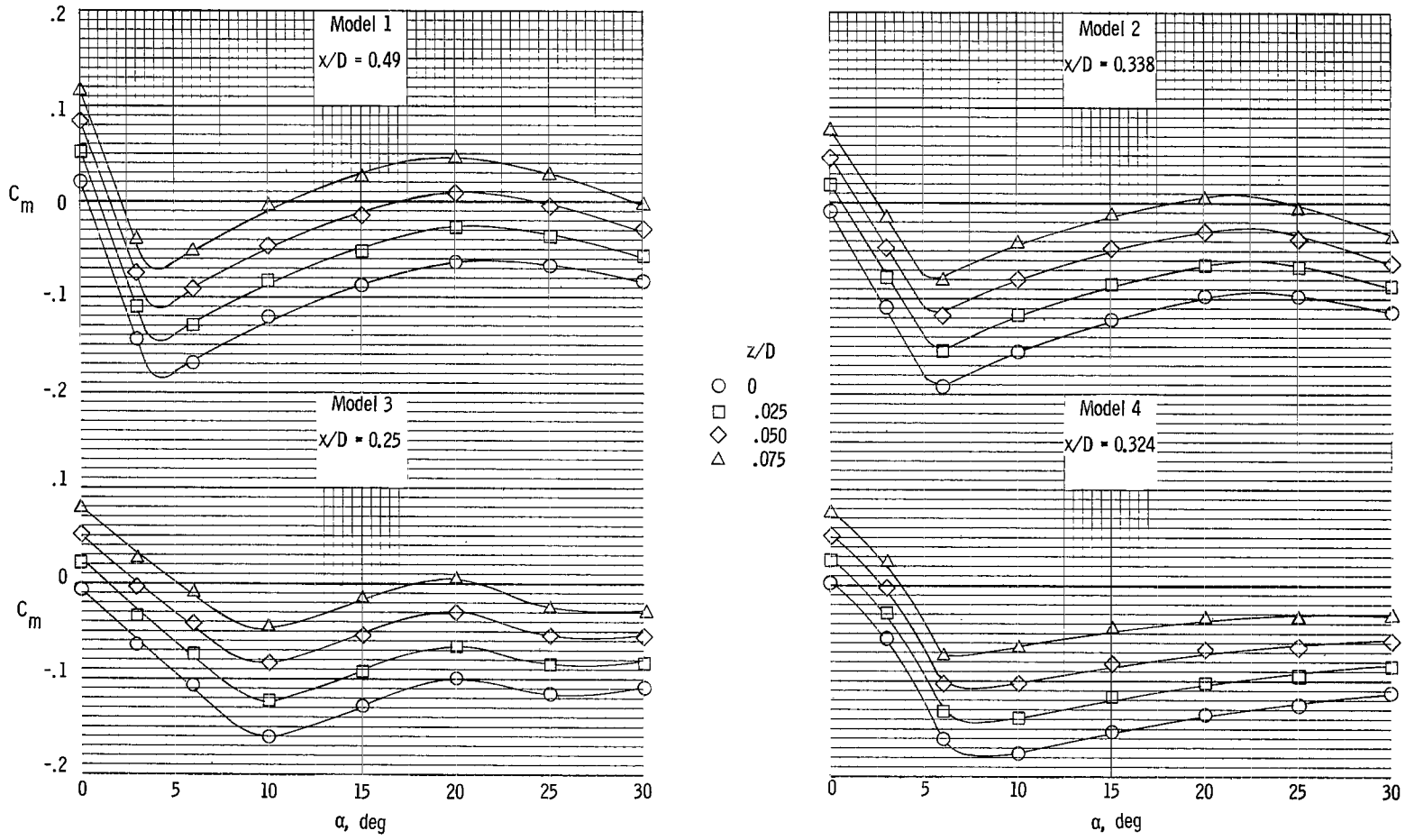

Figure 9.- Effect of varying center-of-gravity location along the vertical axis on pitching-moment coefficient.

2/22/85

"The aeronautical and space activities of the United States shall be conducted so as to contribute . . . to the expansion of human knowledge of phenomena in the atmosphere and space. The Administration shall provide for the widest practicable and appropriate dissemination of information concerning its activities and the results thereof."

—NATIONAL AERONAUTICS AND SPACE ACT OF 1958

NASA SCIENTIFIC AND TECHNICAL PUBLICATIONS

TECHNICAL REPORTS: Scientific and technical information considered important, complete, and a lasting contribution to existing knowledge.

TECHNICAL NOTES: Information less broad in scope but nevertheless of importance as a contribution to existing knowledge.

TECHNICAL MEMORANDUMS: Information receiving limited distribution because of preliminary data, security classification, or other reasons.

CONTRACTOR REPORTS: Technical information generated in connection with a NASA contract or grant and released under NASA auspices.

TECHNICAL TRANSLATIONS: Information published in a foreign language considered to merit NASA distribution in English.

TECHNICAL REPRINTS: Information derived from NASA activities and initially published in the form of journal articles.

SPECIAL PUBLICATIONS: Information derived from or of value to NASA activities but not necessarily reporting the results of individual NASA-programmed scientific efforts. Publications include conference proceedings, monographs, data compilations, handbooks, sourcebooks, and special bibliographies.

Details on the availability of these publications may be obtained from:

SCIENTIFIC AND TECHNICAL INFORMATION DIVISION

NATIONAL AERONAUTICS AND SPACE ADMINISTRATION

Washington, D.C. 20546